NEOPLASIA
www.neoplasia.com

Volume 29 Number xxx Month 2022 pp. 100802

Hoxa11-mediated reduction of cell migration contributes to myeloid sarcoma formation induced by cooperation of *MLL/AF10* with activating *KRAS* mutation in a mouse transplantation model

Hoxa11 in myeloid sarcoma formation

Jen-Fen Fu[a,*]; **Chih-Jen Wen**[b,e]; **Tzung-Hai Yen**[c]; **Lee-Yung Shih**[d,**]

[a] Department of Medical Research, Chang Gung Memorial Hospital, and Graduate Institute of Clinical Medical Sciences, Chang Gung University, Taoyuan, Taiwan
[b] Center for Vascularized Composite Allotransplantation, School of Medicine, Chang Gung Memorial Hospital at Linkou, Chang Gung University, Taoyuan, Taiwan
[c] Department of Nephrology, Chang Gung Memorial Hospital and Chang Gung University, Taipei, Taiwan
[d] Division of Hematology-Oncology, Department of Internal Medicine, Chang Gung Memorial Hospital, Taipei, Taiwan
[e] Brain Research Center, National Tsing Hua University, Hsinchu, Taiwan

Abstract

The molecular mechanism of myeloid sarcoma (MS) formation remains nuclear. Our clinical and mouse model findings from a previous study revealed that cooperation of *KMT2A* (*MLL*) translocation (*MLL*-t) with activating *N-/K-RAS* mutations promoted MS formation in a shorter latency. To improve the understanding of MS formation, in this study, we performed imaging cell trafficking analysis and demonstrated that cells harboring cooperating mutations migrated more slowly to omental adipose tissues and more cells were retained in adipose tissues *in vivo*. Comparison of transcriptome profiling among three pairs of mouse *MLL/AF10(OM-LZ)* leukemia cell lines harboring activating and wild-type *KRAS* identified 77 differentially expressed genes (DEGs) with >1.5-fold change. Functional annotation of these 77 DEGs using Gene Ontology (GO) enrichment analysis followed by cluster analysis revealed that GO terms related to development/differentiation have the highest enrichment score. The roles of *Hoxa10* and *Hoxa11*, two genes which mapped to this cluster, were further characterized. Silencing *Hoxa10* and *Hoxa11* in cells harboring cooperating mutations prolonged the survival and reduced MS formation, respectively, in the recipient mice. Data of imaging cell trafficking as well as competitive engraftment and clonal expansion analyses indicated that silencing or overexpressing *Hoxa11* in mouse leukemia cells affected cell migration and retention in omental adipose tissue. Although silencing *Hoxa11* in leukemia cells did not affect Cxcr4 expression, it resulted in increased transwell migration, motility in confined spaces 3 μm in size, and cell protrusion. Our results revealed that *Hoxa10* plays an important role in survival and *Hoxa11* contributes to MS formation in *MLL*-t acute myeloid leukemia with activating *KRAS* mutation.

Neoplasia (2022) 29, 100802

Keywords: *MLL* translocation, *KRAS* mutation, *Hoxa11*, *Hoxa10*, Myeloid sarcoma, Migration

Introduction

Myeloid sarcoma (MS), previously called chloroma, myeloblastoma, or granulocytic sarcoma, is a rare manifestation of hematologic malignancies presenting as extramedullary soft tissue masses [1,2]. MS can be found in patients either as the only clinical presentation or concomitantly with, before, or after a diagnosis of acute myeloid leukemia (AML), myelodysplastic syndrome, or myeloproliferative neoplasm [1,2]. The incidence of MS in

Abbreviations: AL, acute leukemia; AML, acute myeloid leukemia; APC, allophycocyanin; B6, C57BL/6J; BM, Bone marrow; BP, biological process; CBC, complete blood count; CCK-8, Cell Counting Kit-8; cDNA, complementary DNA; DAVID, Database for Annotation, Visualization, and Integrated Discovery; DEGs, differentially expressed genes; FBS, fetal bovine serum; GO, Gene Ontology; IL, interleukin; ip, intraperitoneally; MF, molecular function; MLL-t, MLL translocations; MS, myeloid sarcoma; nt, nucleotide; PB, peripheral blood; PE, phycoerythrin; qRT-PCR, quantitative reverse transcription polymerase chain reaction; shRNAs, short hairpin RNAs.

* Corresponding author at: Department of Medical Research, Chang Gung Memorial Hospital, 5, Fu-Hsin Street, Kwei-San, Taoyuan 244, Taiwan.

** Corresponding author at: Division of Hematology-Oncology, Department of Internal Medicine, Chang Gung Memorial Hospital, 199 Tung Hwa North Road, Taipei 105, Taiwan.

E-mail addresses: cgfujf@adm.cgmh.org.tw (J.-F. Fu), sly7012@adm.cgmh.org.tw (L.-Y. Shih).

Received 30 August 2021; accepted 18 April 2022

https://doi.org/10.1016/j.neo.2022.100802

patients with AML is approximately 0.8% to 9% [3,4], and it can occur at many sites, the most frequently reported of which are skin, lymph node, gastrointestinal tract, bone, testis, peritoneum, and central nervous system [5-7]. Several chromosomal abnormalities are recurrently detected in patients with MS, including *KMT2A* (*MLL*) translocations (*MLL*-t), t(8;21), inv(16), t(8;16)(p11;p13), monosomy 7, and trisomy 8 [2,5-7]. Patients with AML harboring t(8;21) or *MLL-t* have significantly lower overall survival in the MS group than the non-MS group [8,9]. The most frequently detected genes with mutations in patients with MS are *N-/K-RAS, NPM1,* and *DNMT3A* [10-12]. In a previous study, we found that 3/5 (60%) of patients with AML and *MLL/AF10* and *N-/K-RAS* mutations had MS formation [13]. Using a retroviral transduction/transplantation mouse model, we demonstrated that cooperation of *MLL/AF10* with activating *KRAS* ($KRAS^{G12C}$) induced MS formation in a shorter latency [13]. Our results supported that *MLL-t* and *KRAS* mutations are associated with MS formation, and additionally, MS formation is associated with shorter survival.

The molecular mechanism of MS formation remains unclear. Among the chromosomal abnormalities frequently detected in patients with MS, *MLL*-t and t(8;16)(p11;p13) involve genes with epigenetic regulating activities. *MLL* encodes a histone H3 lysine 4 methyltransferase that is essential for regulating gene expression during early development and hematopoiesis. Translocations of *MLL* lead to misregulation of *MLL* downstream genes, such as *HOXA7–HOXA10*, and subsequently, impair hematopoietic lineage commitment and induce leukemia development [14,15]. Cells from the human leukemia cell line THP-1, possessing *MLL/AF9* and activating *NRAS*, have high expression levels of *HOXA11, HOXA10, HOXA7*, and *HOXA4*. These genes were downregulated during phorbol 12-myristate 13-acetate-induced monocyte-macrophage differentiation [16]. The t(8;16)(p11;p13) translocation results in the fusion of *MYST3* and *CREBBP*, both of which exhibit histone acetyltransferase activity. Gene expression profile analysis of AML cases with t(8;16)(p11;p13) revealed that they were clustered near those with *MLL-t* and highly expressed *HOXA11, HOXA10, RET, PERP*, and *GGA2* [17]. Increased expression of *HOXA10* and *HOXA11* was reported in both types of AML. *HOXA10* expression in AML is associated with poor prognosis [18,19]. Additionally, *Hoxa10* overexpression-induced AML was confirmed using a mouse model [20]. In contrast, the t(7;11)(p15;p15) translocation, which results in the fusion of *NUP98* and *HOXA11*, was identified in patients with AML, chronic myeloid leukemia, and juvenile myelomonocytic leukemia [21,22], suggesting that *Hoxa11* is closely related to leukemogenesis. Whether these two genes are involved in MS formation has not been investigated.

To improve the understanding of MS formation, in this study, we compared the transcriptome profiling between mouse *MLL/AF10(OM-LZ)* leukemia cells harboring wild-type and oncogenic *KRAS* and discovered that *Hoxa10* and *Hoxa11* were differentially expressed. Additionally, the functions of *Hoxa10* and *Hoxa11* in survival and MS formation were investigated using a mouse model, and the roles of *Hoxa11* in cell migration, retention, motility, and protrusion formation were examined.

Materials and methods

Cell lines and cell culture conditions

Mouse *MLL/AF10* leukemia cell lines have been generated by retroviral transduction of *MLL/AF10(OM-LZ)* and wild-type ($KRAS^{wt}$) or activating *KRAS* ($KRAS^{G12C}$) to 5-fluorouracil-enriched C57BL/6 (B6; National Laboratory Animal Center, Taiwan) mouse bone marrow (BM) cells in our previous studies [13,23,24]. Of these mouse leukemia cell lines, 12G cells harbor *MLL/AF10(OM-LZ)* solely, AK2G and AK3G cells harbor *MLL/AF10(OM-LZ)* and $KRAS^{G12C}$, and AKw1G cells harbor *MLL/AF10(OM-LZ)* and $KRAS^{wt}$. Mouse leukemia cell lines were maintained in RPMI 1640 medium (Gibco, Grand Island, NY, USA) containing 20% fetal bovine serum (FBS; Hyclone, Logan, UT, USA), 2 mM L-glutamine, 100 μM 2-mercaptoethanol, and 10 ng/ml interleukin-3 (R&D Systems, Minneapolis, MN, USA).

Imaging cell trafficking analysis

CellVue NIR815-labeled cells were prepared according to the manufacturer's instructions (LI-CORE Biosciences, Lincoln, NE, USA). Briefly, leukemia cells were washed using medium without FBS and resuspended in diluent C reagent containing CellVue NIR815 dye (LI-CORE) at a final concentration of 10^{-5} M for 5 min. The dye uptake reaction was stopped by adding an equal volume of FBS to the cell suspension. Labeled cells were washed to remove the unincorporated CellVue NIR815 dye and then imaged using Pearl Imager (LI-CORE) or by fluorescence microscopy (TissueGnostics GmbH, Vienna, Austria) to ensure successful labeling. The labeled cells were intraperitoneally (ip) injected into sublethally irradiated B6 mice (1×10^6 cells/mouse). Mice injected with unlabeled cells served as blank controls. *In vivo* fluorescence images of the transplanted mice were collected using Pearl Imager at 5 min, 1.5 h, 24 h, 7 days, 25 days, and 32 days. During the imaging period, mice were anesthetized with 2.5% isoflurane gas in the oxygen flow (1.5 l/min). In all imaging experiments, reproducibility was confirmed with 3–5 independent mice. The fluorescent signals of organ biopsies from transplanted mice were detected using Xenogen IVIS Spectrum (Caliper Life Science, Hopkinton, MA, USA) or Pearl Imager. Organ and tissue biopsies were also formaldehyde-fixed, paraffin-embedded, sectioned, and stained by hematoxylin and eosin staining reagents according to standard protocols.

Microarray analysis and Gene Ontology (GO) enrichment analysis

Trizol reagent (Invitrogen, Carlsbad, CA, USA) was used to extract total RNA of leukemia cells. The RNA was amplified, labeled, and then hybridized with a mouse genome 430A Array chip (12G vs. AK3G), 430 2.0 Array chip (12G vs. AK2G), or Clariom D Array chip (AKw1G vs. AK3G) (Affymetrix, Santa Clara, CA, USA) according to the manufacturer's instructions. This procedure was performed by the staff of the Genomic Medicine Research Core Laboratory at Chang Gung Memorial Hospital in Linkou, Taiwan. The microarray data are available at the NCBI GEO website (accession numbers: GSE82156 and GSE134586) [24,25]. Transcriptome Analysis Console (TAC) software 4.0 (Affymetrix) was used for differential expression analysis. Heatmaps were generated using TreeView Cluster 3.0 (http://bonsai.hgc.jp/~mdehoon/software/cluster/) and JavaView v1.1.6r4 (http://www.javaview.de). Differentially expressed genes (DEGs) with more than 1.5-fold change between paired leukemia cell lines were functionally annotated with Gene Ontology (GO) enrichment analysis using online Database for Annotation, Visualization, and Integrated Discovery (DAVID) v6.8 annotation tools (https://david.ncifcrf.gov/). Statistical significance was evaluated using Fisher's exact test and adjusted by Bonferroni correction for multiple testing. The GO biological process (GO_BP) terms with $P < 0.05$ were considered statistically significant.

Reverse transcription-quantitative polymerase chain reaction (RT-qPCR)

Total RNA of mouse leukemia cells was reverse transcribed into complementary DNA (cDNA) using random hexamers and Superscript II reverse transcriptase (Life Technologies, Rockville, MD, USA) according to the manufacturer's protocol. Quantitative PCR was performed using SYBR Green PCR master mix and analyzed using an ABI Prism 7900 system (Applied Biosystems, Foster City, CA, USA). The primer sets were 5′-GAA AAC CTC GCT TCC TCC GA-3′ and 5′-ATA AGG GCA GCG CTT TTT GC-3′ for mouse *Hoxa11*, 5′-CCA AAG GCG AAA ATG CAG CC-3′ and 5′-CGT CTG GTG CTT CGT GTA AG-3′ for *Hoxa10*, and 5′-TTC ACC

ACC ATG GAG AAG GC-3′ and 5′-GGC ATG GAC TGT GGT CAT GA-3′ for *Gapdh*. The thermal cycling conditions were as follows: 95°C for 2 min, followed by 40 cycles of 95°C for 15 s and 65°C for 30 s. The gene expression level of the target gene was normalized by the housekeeping gene *Gapdh*. Fold change was calculated as $2^{-\Delta\Delta Ct}$ [26].

Gene knockdown by short hairpin RNA (shRNA)

To generate stable *Hoxa10* and *Hoxa11* knockdown cell lines, AK3G cells were infected with a lentivirus-expressing shRNA against *Hoxa10* (The RNAi Consortium shRNA clone numbers TRCN0000012515 and TRCN0000012516) or against *Hoxa11* (TRCN0000070753 and TRCN0000070755) at a multiplicity of infection of one. The lentiviruses were obtained from the National RNAi Core Facility at the Institute of Molecular Biology/Genomic Research Center, Academia Sinica, Taiwan. Infected cells were selected in RPMI medium containing puromycin (2.5 μg/ml) for 2 weeks. AK3G cells stably transfected with blank lentiviral vector pLKO.1-emptyT or pLKO_TRC025 were used as negative controls.

Western blotting

Western blotting was performed as described previously [13]. Twenty micrograms of total protein lysate was loaded in each lane. The primary antibody against mouse Hoxa10 (1:5000, GWB-CEOCD3) was obtained from GenWay (San Diego, CA, USA), whereas those for Hoxa11 (1:5000, NBP1-80228) and β-actin (1:10000, sc-47778) were obtained from Novus Biologicals (Littleton, CO, USA) and Santa Cruz Biotechnology (Santa Cruz, CA, USA), respectively. The horse radish peroxidase (HRP)-conjugated secondary antibody (1:10000, C04001) was obtained from Croyez Bioscience (Taipei, Taiwan). Chemiluminescence was generated using a Western Lightning Plus ECL Kit (Perkin Elmer, Skovlunde, Denmark) and captured using X-ray film or Analytik Jena^{TM} UVP ChemStudio PLUS and analyzed by VisionWorks Touch Software 9.0 (Analytik Jena US LLC, Upland, CA, USA).

BM transplantation assay

The BM transplantation assay has been reported previously [25,27]. Briefly, leukemia cells were ip injected into male B6 mice (1×10^6 cells/mouse) that received either a sublethal dose of γ-irradiation (5.25 Gy) (AKw1G and AK5G, n = 5 each; AK3G-shV and AK3G-shH10-2, n = 10 each) or no irradiation (AK3G-shV and AK3G-shH11-2, n = 10 each). Mice ip injected with normal saline (n = 5) served as a blank control. Mouse complete blood count of peripheral blood was assessed weekly by hemocytometry using a Hemavet 950 (Drew Scientific, Oxford, CT, USA) or BC-5000 (Mindray, Shenzhen, China). Physical examination was performed daily. Mice were sacrificed at the moribund state, which was characterized by leukocytosis, with hunched posture, weakness, shortness of breath, and 20% body weight loss. BM, peripheral blood, ascites, organs, and tumor masses were collected and weighed.

Competitive engraftment and clonal expansion assay

The competitive engraftment and clonal expansion assay has been described previously [25,27]. Briefly, paired cells (AK3G-shV vs. AK3G-shH11-2 and 12G-V vs. 12G-H11-1) were mixed at a ratio of 1:1 and then ip injected into B6 mice (2×10^6 cells/mouse). The mice were sacrificed 1 day or 4 weeks post-transplantation (n = 3 for each time point). Mouse omental adipose tissue around the splenic and gastric veins or gonadal adipose tissue was collected and used to extract genomic DNA. To amplify the region spanning the shRNA cloning site from genomic DNA, PCR was performed using the LKO 5′ primer 5′-TGG ACT ATC ATA TGC TTA CCG-3′ in combination with the LKO 3′ primer 5′-GTC TGT TGC TAT TAT GTC TAC-3′. The LKO 5′ primer was also used for sequencing PCR products. The peak height of the 79th nucleotide (G for AK3G-shV and C for AK3G-shH11-2) was measured. To amplify DNA fragments of the pMSCVpuro vector (from 12G-V) or the region spanning the pMSCVpuro-*Hoxa11* junction (from 12G-H11-1) from genomic DNA, PCR was performed using the MSCV 5′ primer 5′-CCC TTG AAC CTC CTC GTT CAG CC-3′ with the MSCV 3′ primer 5′-GAG ACG TGC TAC TTC CAT TTG TC-3′ and the *Hoxa11* primer 5′-GAG TAG CAG TGG GCC AGA TTG C-3′. The MSCV 5′ primer was used for sequencing PCR products. The peak height of the 62nd nucleotide (C for 12G-H11 and G for 12G-V) was measured. The (C / C + G) peak height ratio was converted to the cell ratio (12G-H11 / 12G-H11 + 12G-V or AK3G-shH11 / AK3G-shV + AK3G-shH11) by aligning to the standard curve. The standard curve was generated by the same method described above using genomic DNA obtained from premixed paired cells in ratios of 10:0, 8:2, 6:4, 4:6, 2:8, and 0:10.

Flow cytometry analysis

To detect CXC chemokine receptor-4 (Cxcr4) expression, leukemia cells were incubated with allophycocyanin (APC)-conjugated anti-mouse CD184 (Cxcr4) antibody (0.5 μg per 10^6 cells in 100 μl volume, #146507; BioLegend, San Diego, CA, USA). Cells incubated with an isotype antibody (0.5 μg per 10^6 cells in 100 μl volume, #400612; BioLegend) served as a negative control. Data were acquired using a FACS Canto II flow cytometer (Becton-Dickinson, San Jose, CA, USA) and analyzed using FlowJo v10.4 software (Tree Star Software, San Carlos, CA, USA).

Transwell migration assay

Cells (1×10^5) were added to the insert of a 24-well Transwell plate (5-μm pore size; Corning Costar, Cambridge, MA, USA), and RPMI 1640 medium with stromal derived factor-1 (SDF-1) (150 ng/ml; PeproTech, Rocky Hill, NJ, USA) was added to the bottom chamber. After 6-h incubation, the cells in the insert and bottom chamber were counted using a hemacytometer. The values shown are expressed as the mean ± standard deviation (SD) of three independent experiments.

Cell motility and protrusion in confined spaces

To observe leukemia cell motility and protrusion formation in confined spaces (3 μm in size), the polydimethylsiloxane (PDMS) slab–based approach [28] was performed with some modifications. Briefly, a PDMS layer (SYLGARD 184 Kit; Dow Corning, Midland, MI, USA) was polymerized in a 30-mm glass-bottom culture dish (GeneDireX, Taiwan). An 8-mm hole was made by putting a polystyrene cloning cylinder (Sigma-Aldrich, St Louis, MO, USA) into the PDMS during polymerization. Cells were stained using a Celltrace Far Red Cell Proliferation Kit (Thermo Fisher, Waltham, MA, USA) according to the manufacturer's instructions. A 50-μl cell suspension (5×10^4) and 0.5 μl of latex beads (10%) (3-μm in diameter; SI-LB30, Sigma-Aldrich) were mixed thoroughly and pipetted into the hole. The cells and beads were moved into the space underneath the PDMS slab by lifting it using a pipette tip. The dish was then placed on the stage of a ZEISS Axiovert 200M inverted fluorescence microscope (Carl Zeiss AG, Oberkochen, Germany) equipped with a digital camera. After 30 min to ensure that the beads were holding tightly to create a confined space between the PDMS slab and the dish bottom, images were acquired every 6 s for 20 min. To observe the directional migration and protrusion of cells in response to SDF-1, 100 μl of SDF-1 (150 ng/ml in RPMI 1640 medium) was added to the hole, and after a 10-min incubation, the images were acquired every 6 s for 20 min.

Table 1

Survival and extramedullary myeloid sarcoma formation in the recipient mice.

	AKw1G	AK5G	P_value	AK3G-shV	AK3G-shH10-2	P_value	AK3G-shV	AK3G-shH11-2	P_value
Mouse number	5	5		10	10		10	10	
Survival (range) (days)*	88 (83->120)	77 (57-84)	0.0332	55 (44-60)	65.5 (59-80)	<0.001	64 (54-83)	65 (48-77)	0.4738
MS occurrence (%)#	0%	100%	0.0079	90%	89%	1.0000	100%	100%	1.0000
Gonad (g)*	0.94	1.06	0.1202	1.24	0.88	0.1480	1.41	1.15	0.3404
Gonad/TBW (%)*	3.24%	3.57%	0.3479	4.7%	4%	0.1237	4.3%	4%	0.5119
OM (g)*	0.78	1.86	0.0227				2.01	1.01	0.0057
OM/TBW (%)*	3.02%	5.82%	0.0213				6.5%	3.5%	0.0045
GI-OM (g)*				3.82	3.32	0.9927			
GI-OM/TBW (%)*				13.9%	13.6%	0.9741			
Ascites (%)#	0%	100%	<0.001	50%	30%	0.6500	80%	10%	0.0050

* T test or log-rank test
# Fisher's exact test

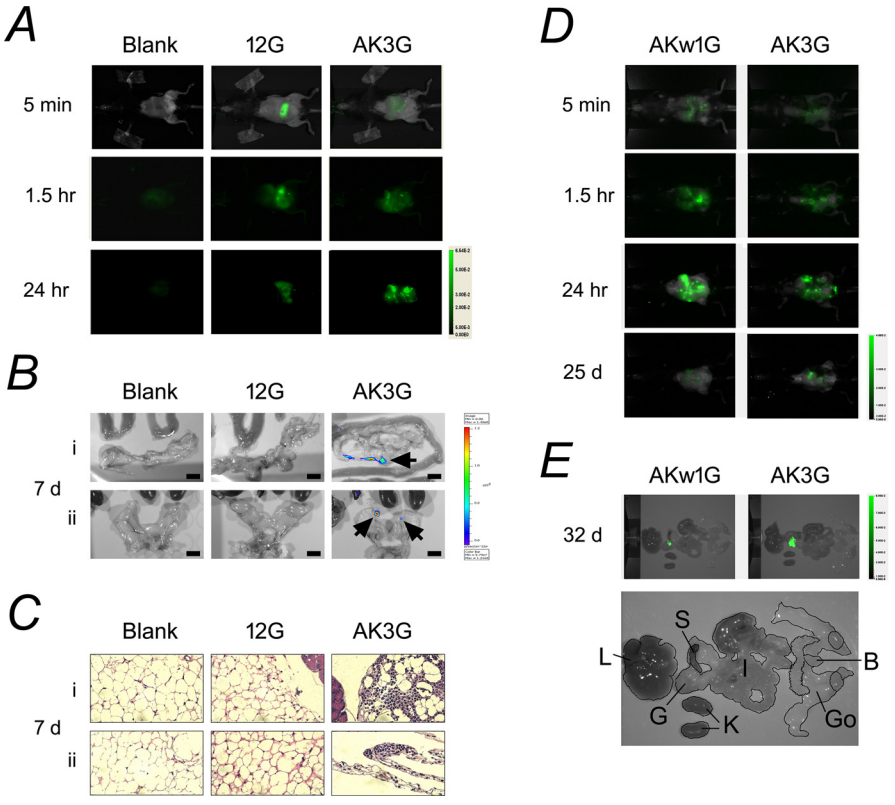

Fig. 1. Migration and retention of AK3G cells at extramedullary sites. (A) Imaging analysis of mice ip injected with normal saline (blank) or 1:1 mixed 12G and AK3G cells by Peral Imager at indicated time points. CellVue NIR815-labeled mice were under anesthesia during image capture. (B) Imaging analysis of excised omental (i) and gonadal adipose tissue from blank, 12G, and AK3G mice by Xenogen IVIS Spectrum 7 days post-transplantation. Arrows indicate fluorescent signals. (C) Histologic features of omental (i) and gonadal (ii) adipose tissues obtained from blank, 12G, and AK3G mice 7 days post-transplantation (× 40, H&E stain). (D) Imaging analysis of mice ip injected with CellVue NIR815-labeled AKw1G or AK3G cells by Peral Imager at indicated time points. (E) Imaging analysis of excised organs from AKw1G and AK3G mice by Pearl Imager 32 days post-transplantation (upper panel). The arrangement of organs is shown in the lower panel. L, liver; S, spleen; G, stomach; I, intestine; B, bladder; Go, gonad. Color bars (A, B, D, E) indicate the total fluorescence radiant efficiency.

Ethical requirements

All animal experiments were performed according to the protocol approved by the Animal Research Committee of Chang Gung Memorial Hospital (IACUC No. 2015033001).

Statistical analyses

The statistical significance of differences in gene expression levels of the two groups based on cDNA microarray data was compared by the Mann–Whitney test. Survival analysis was conducted according to the

A

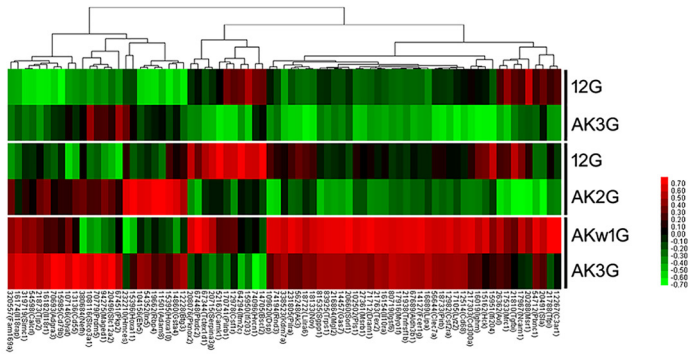

B

Term	*P* Value	Genes
GO:0002376~immune system process	8.25E-05	CD79B, CD55, CSF1R, HCK, CD300A, AXL, SERPINA3G, PIRB, MSRB1
GO:0006954~inflammatory response	2.77E-04	ADAM8, CSF1R, HCK, CLEC7A, AXL, C3AR1, TNFRSF1B, LIPA
GO:0045087~innate immune response	6.83E-04	CD55, CSF1R, IGHM, HCK, FCER1G, CLEC7A, AXL, MSRB1
GO:0007166~cell surface receptor signaling pathway	0.00131	ADGRA3, CD79B, CALCRL, FCER1G, NCAM1, TNFRSF1B
GO:0060065~uterus development	0.00222	HOXA10, RBP4, HOXA11
GO:0007169~transmembrane receptor protein tyrosine kinase signaling pathway	0.00609	CSF1R, HCK, PILRB1, PILRA
GO:0002062~chondrocyte differentiation	0.01260	NOV, TRPS1, TGFBI
GO:0006898~receptor-mediated endocytosis	0.02085	MSR1, CD300A, MRC1
GO:0045110~intermediate filament bundle assembly	0.02203	PKP2, NEFH
GO:0086073~bundle of His cell-Purkinje myocyte adhesion involved in cell communication	0.02203	PKP2, DSP

C

Annotation Cluster 1	Enrichment Score: 1.52		
	Term	*P* Value	Genes
	GO:0060065~uterus development	0.00222	HOXA10, RBP4, HOXA11
	GO:0008584~male gonad development	0.06482	HOXA10, RBP4, HOXA11
	GO:0007283~spermatogenesis	0.19151	HOXA10, RBP4, HOXA11, AXL
Annotation Cluster 2	Enrichment Score: 0.46		
	Term	*P* Value	Genes
	GO:0016310~phosphorylation	0.19124	CSF1R, HCK, AXL, AK3, CAMK1
	GO:0030154~cell differentiation	0.32753	ETV5, HCK, AXL, CAMK1, GAS7
	GO:0006468~protein phosphorylation	0.36024	CSF1R, HCK, AXL, CAMK1
	GO:0043066~negative regulation of apoptotic process	0.62468	CSF1R, HCK, AXL

Fig. 2. Upregulation of *Hoxa10* and *Hoxa11* in *MLL/AF10* cells harboring *KRAS*^{G12C}. (A) Heat map representing the relative gene expression levels of 77 shared DEGs between paired cell lines based on cDNA microarray data. Two Affymetrix chips were used in paired cell lines: the 430A (12G vs. AK3G and 12G vs. AK2G) and the Clariom D (AKw1G vs. AK3G). Raw values were log2-transformed and centered relative to the median. A heat map was obtained using Cluster 3.0 and Java TreeView v1.1.6r4. The color bar depicts the color contrast level of the heat map. Red and green indicate high and low expression levels, respectively. (B) Top 10 enriched GO_BP terms for 77 DEGs. All GO terms listed in the table show significant enrichment (all $P < 0.05$). Red and blue indicate genes that are upregulated or downregulated, respectively, in *MLL/AF10* cells harboring *KRAS*^{G12C}. (C) Two clusters of redundant annotation GO_BP terms. GO enrichment and clustering analyses were performed using online DAVID v6.8 annotation tools.

Kaplan–Meier method. The statistical significance of differences in organ weight and transwell migration was assessed using the Student's t-test. All statistical analyses were performed using SPSS software version 20.0 for Windows (IBM Corp., Armonk, NY, USA). A *P* value less than 0.05 indicated statistical significance.

Results

Survival and MS formation in mice transplanted with MLL/AF10 leukemia cells harboring wild-type or mutant KRAS

The mouse *MLL/AF10(OM-LZ)* leukemia cell line (12G) and *MLL/AF10(OM-LZ)* cells harboring *KRAS*^{G12C} (AK2G, AK3G, and AK5G) or *KRAS*^{wt} (AKw1G) were generated by retroviral transduction in our previous studies [13,23,24] and in this study (Supplementary Figure 1*A*). Our previous studies have demonstrated that mice transplanted with AK2G or AK3G cells had shorter survival compared with those transplanted with 12G. Additionally, 100% of the AK2G and AK3G mice, but not 12G mice, formed MS in omental-mesentery, gonadal, and subcutaneous adipose tissues [13]. In this study, we further demonstrated that mice transplanted with AK5G cells had shorter survival than those injected with AKw1G cells (Supplementary Figure 1*B*). Like AK2G and AK3G mice, AK5G mice, but not AKw1G mice, had significant MS formation in omental-mesentery adipose tissues (Supplementary Figure 1*C*; Table 1).

In vivo *imaging to monitor cell trafficking*

To investigate the process of MS formation in adipose tissues, *in vivo* imaging analysis was performed to monitor leukemia cell trafficking. The results showed that in mice ip injected with CellVue NIR815-labeled AK3G cells, dispersed fluorescent signals in the peritoneal cavities gradually condensed after 1.5 h, with the signals gaining strength 24 h post-transplantation (Fig. 1*A*, right column). Excised organs from AK3G mice 7 days post-transplantation showed that the fluorescent signals were mainly localized in the adipose tissue around the gastric and splenic veins (omental adipose tissue) (Fig. 1*B*-i, right column) or the epididymis and testis

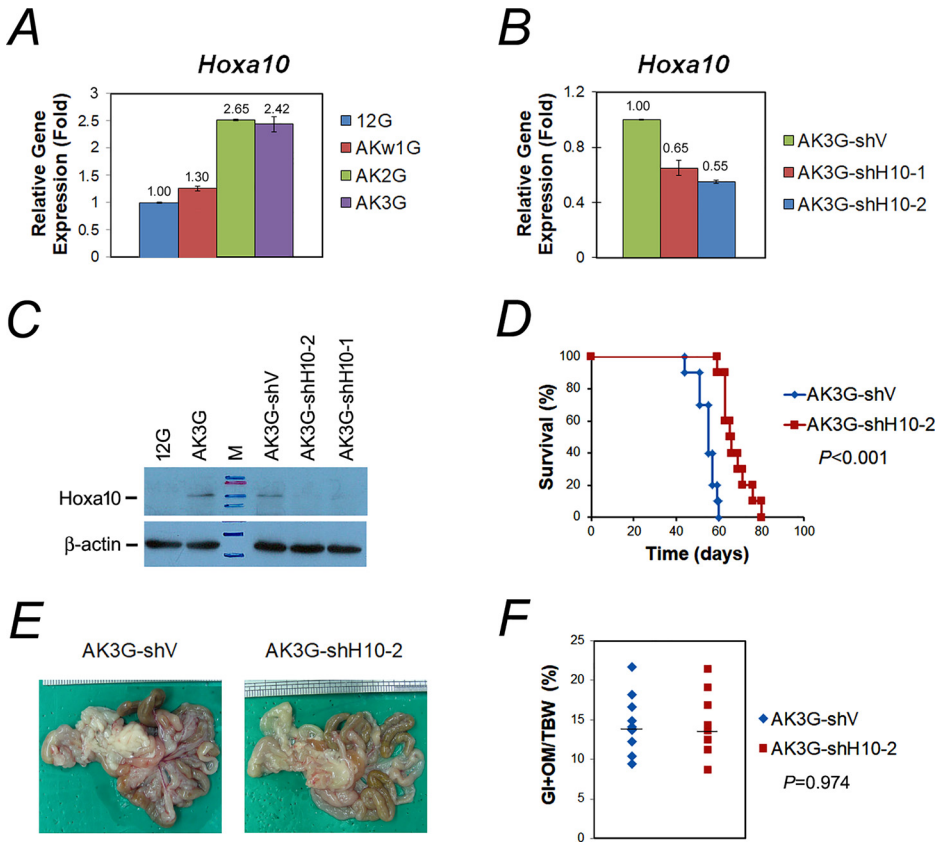

Fig. 3. Silencing *Hoxa10* of AK3G cells prolonged survival of leukemic mice. (A, B) The mRNA level of Hoxa10 in 12G, AKw1G, AK2G, and AK3G cells (A), and AK3G-shV, AK3G-shH10-1, and AK3G-shH10-2 cells (B) were determined by RT-qPCR analysis. Data shown are representative of three independent experiments. Error bars indicate SD of the mean. Fold changes are indicated above the bars. (C) The protein level of Hoxa10 in AK3G-shV and AK3G-shH10-2 cells was determined by Western blotting. β-actin was used as the loading control. (D) Kaplan–Meier survival curves of sublethally γ-irradiated mice ip injected with AK3G-shV or AK3G-shH10-2 cells. A P value less than 0.05 indicates statistical significance. (E) Gross view of excised gastrointestinal tract and omental-mesentery (GI-OM) adipose tissue from representative AK3G-shV and AK3G-shH10-2 mice. (F) Aligned dot plot showing the percentage weight of GI-OM adipose tissue over the total body weight of AK3G-shV and AK3G-shH10-2 mice. Horizontal lines represent the median, which was not statistically different between AK3G-shV and AK3G-shH10-2 mice (13.9% vs. 13.6%, respectively; P = 0.974).

(gonadal adipose tissue) (Fig. 1*B*-ii, right column). Histologic examination of omental (Fig. 1*C*-i, right column) and gonadal adipose tissues (Fig. 1*C*-ii, right column) from AK3G mice revealed that leukemia cells aggregated in adipocyte septa. In contrast, the fluorescent signals in mice transplanted with 12G cells condensed within 5 min. The fluorescent signals then gradually decreased after 1.5 h, and only rare fluorescent signals were detected 24 h post-transplantation (Fig. 1*A*, middle column). Few fluorescent signals and leukemia cells were detected in the corresponding tissues from 12G-injected but not blank mice (Fig. 1, *A*–*C* middle and left columns).

The fluorescent signals in mice transplanted with AKw1G cells were similar to that of AK3G cells but with a stronger intensity during the first day. However, significantly fewer fluorescent signals were observed *in vivo* and in the excised omental adipose tissue compared to that of AK3G mice 25 days and 32 days post-transplantation, respectively (Fig. 1, *D*–*E*). These results indicated that, compared to AKw1G cells, AK3G cells exhibited slower cell migration to and longtime retention in adipose tissue. Those cells retained in adipose tissue were proliferating and eventually formed MS.

Identification of DEGs and GO enrichment analysis

To identify the genes responsible for MS formation by leukemia cells in adipose tissues, we compared transcriptome profiling between three pairs of *MLL/AF10(OM-LZ)* leukemia cells harboring $KRAS^{wt}$ and $KRAS^{G12C}$ (12G vs. AK3G, 12G vs. AK2G, and AKw1G vs. AK3G) using cDNA microarray data. Seventy-seven shared DEGs with more than 1.5-fold change were identified, consisting of 25 upregulated and 52 downregulated genes in AK2G/AK3G cells (Fig. 2A). Functional annotation of the 77 DEGs was performed using DAVID Bioinformatics Resources v6.8. The top 10 GO_BP terms overrepresented in these 77 DEGs included three related to immune/inflammatory responses, two related to receptor signaling, two related to development/differentiation, one related to endocytosis, one related to intermediate filament bundle assembly, and one related to myocyte adhesion-cell communication (all $P < 0.05$) (Fig. 2B). Clustering analysis of all GO_BP terms showed that the terms related to development were the most enriched (Fig. 2*C*). Among the genes mapped to development, *Hoxa10* and *Hoxa11* were upregulated in AK2G and AK3G cells (Fig. 2*A*). Since high expression of *HOXA10* and *HOXA11* was observed in AML with *MLL*-t or t(8;16)(p11;p13), and these two types of AML are frequently associated with MS formation(13, 17), we selected *Hoxa10* and *Hoxa11* for further investigation of their roles in MS formation and survival.

Involvement of Hoxa10 in survival

To confirm the differential expression of *Hoxa10* in *MLL/AF10(OM-LZ)* leukemia cells based on cDNA microarray data, RT-qPCR analysis was performed and confirmed that AK2G and AK3G cells have higher expression

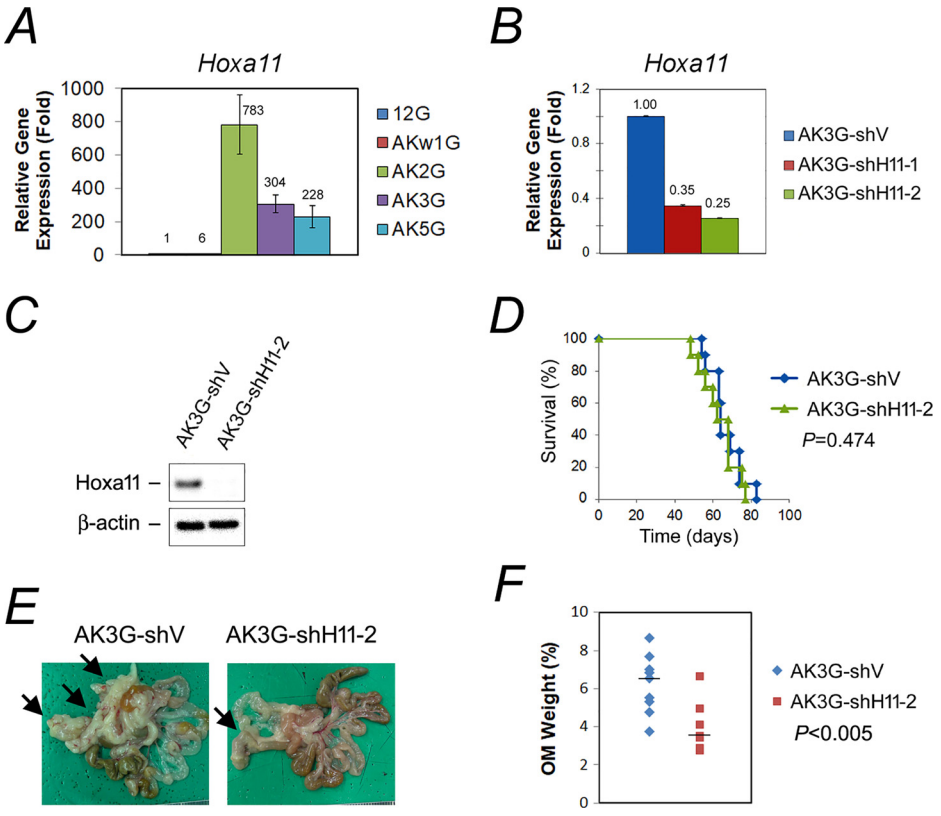

Fig. 4. Silencing *Hoxa11* of AK3G cells reduced MS formation in omental adipose tissue in vivo. (A, B) The mRNA level of Hoxa11 in 12G, AKw1G, AK2G, AK3G, and AK5G cells (A), and AK3G-shV, AK3G-shH11-1, and AK3G-shH11-2 cells (B) were determined by RT-qPCR analysis. Data shown are representative of three independent experiments. Error bars indicate SD of the mean. Fold changes are indicated above the bars. (C) The protein level of Hoxa11 in AK3G-shV and AK3G-shHoxa11-2 cells was determined by Western blotting. β-actin was used as the loading control. (D) Kaplan–Meier survival curves of sublethally γ-irradiated mice ip injected with AK3G-shV or AK3G-shH11-2 cells. The difference was not statistically significant (P =0.474). (E) Gross view of excised GI-OM adipose tissue from AK3G-shV and AK3G-shH11-2 mice. Arrows indicate tumor masses. (F) Aligned dot plot showing the percentage weight of OM adipose tissue over the total body weight of AK3G-shV and AK3G-shH11-2 mice. Horizontal lines represent the median, which was statistically different between AK3G-shV and AK3G-shH11-2 mice (6.5% vs. 3.5%, respectively; P < 0.005).

levels of *Hoxa10* compared to 12G and AKw1G cells (Fig. 3*A*). To investigate the role of *Hoxa10*, we first generated stable *Hoxa10* knockdown AK3G cells by lentiviral transduction of shRNAs targeting *Hoxa10*. Measurement of *Hoxa10* mRNA levels of lentiviral-transduced AK3G-shH10-1 and AK3G-shH10-2 cells revealed 35% and 45% reduction, respectively, compared to control AK3G-shV cells (Fig. 3*B*). The successful generation of *Hoxa10* knockdown clones was further confirmed by Western blotting (Fig. 3*C*). Data of the BM transplantation assay revealed significantly longer survival of the mice transplanted with AK3G-shH10-2 cells than those with AK3G-shV cells (median 65.5 days vs. 55 days, respectively; $P < 0.001$) (Fig. 3*D* and Table 1). However, no differences in MS formation in omental-mesentery or gonadal adipose tissues were observed between the mice transplanted with AK3G-shH10-2 cells and control AK3G-shV cells (Fig. 3, *E–F* and Table 1). These results indicated that the upregulation of *Hoxa10* by cooperation of *MLL/AF10(OM-LZ)* with activating *KRAS* accelerates disease progression but not MS formation.

Involvement of Hoxa11 in MS formation

RT-qPCR analysis confirmed the induction of *Hoxa11* expression in AK2G, AK3G, and AK5G cells compared to 12G and AKw1G cells (Fig. 4*A*). Stable *Hoxa11* knockdown AK3G clones (AK3G-shH11-1 and AK3G-shH11-2) were generated by lentiviral transduction of shRNAs targeting *Hoxa11* to AK3G cells. Compared to control AK3G-shV cells, the reductions of *Hoxa11* mRNA and protein levels in AK3G-shH11-1 and AK3G-shH11-2 cells were confirmed by RT-qPCR and Western blotting, respectively (Fig. 4, *B–C*). It is of note that, although the *Hoxa11* knockdown efficiencies of the cells are significant (35% in AK3G-shH11-1 and 25% in AK3G-shH11-2 cells compared to AK3G-shV cells), the expression level of *Hoxa11* in AK3G-shH11-2 cells did not drop to the level of no expression as that of 12G or AKw1G cells (Fig. 4, *A–B*). Data of the BM transplantation assay revealed no significant differences in survival between mice transplanted with AK3G-shV and AK3G-shH11-2 cells (Fig. 4*D* and Table 1). Nevertheless, compared to AK3G-shV mice, AK3G-shH11-2 mice had significantly reduced MS size in omental adipose tissue (Fig. 4, *E–F* and Table 1). Our results indicated that the induction of *Hoxa11* expression by cooperation of *MLL/AF10(OM-LZ)* with $KRAS^{G12C}$ contributes to MS formation.

Hoxa11 in leukemia cell migration and retention in vivo *and in vitro*

In vivo imaging cell trafficking analysis of mice injected with a 1:1 premix of AK3G-shH11-2 and AK3G-shV cells, using CellVue-NIR815 to label cells of one of the two cell lines at a time, revealed that the fluorescent signals of AK3G-shH11-2 cells rapidly condensed within 5 min, were maintained for 1.5 h, and then decreased 24 h post-transplantation (Fig. 5*A*, right column). In contrast, the fluorescent signals of AK3G-shV cells condensed after 1.5 h and were maintained for 24 h post-transplantation (Fig. 5*A*, left column). Excised organs derived from mice 7 days post-transplantation showed that

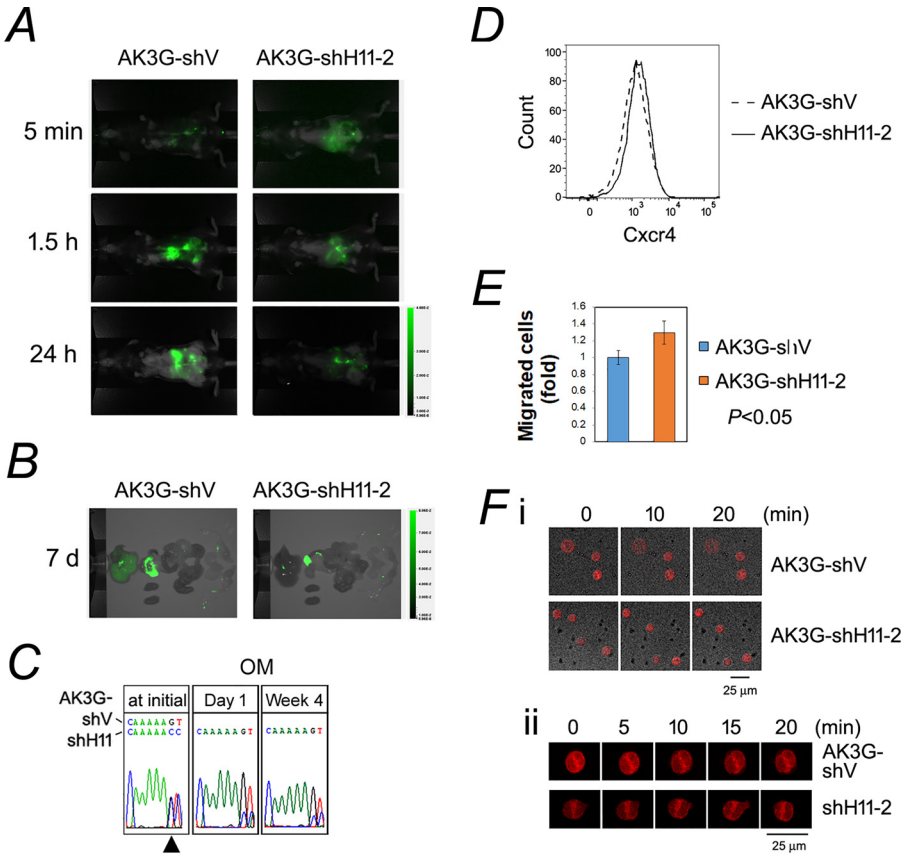

Fig. 5. Silencing *Hoxa11* of AK3G cells enhanced cell migration and reduced cell retention in omental adipose tissue. (A) Imaging cell trafficking analysis of mice ip injected with CellVue NIR815-labeled AK3G-shV or AK3G-shH11-2 cells by Peral Imager at indicated time points. Mice were under anesthesia during image capture. (B) Imaging analysis of excised organs from AK3G-shV and AK3G-shH11-2 mice 7 days post-transplantation by Pearl Imager. Color bars (A, B) indicate the total fluorescence radiant efficiency. (C) Competitive engraftment and clonal expansion analysis of AK3G-shV and AK3G-shH11-2 cells in the omental (OM) adipose tissue of recipient mice on day 1 and week 4. AK3G-shV and AK3G-shH11-2 cells were initially mixed at a 1:1 ratio (1×10^6 cells/cell line). The arrowhead indicates the 79th nucleotide (C for AK3G-shH11-2 and G for AK3G-shV). (D) Flow cytometric analysis of Cxcr4 receptor protein levels of AK3G-shV and AK3G-shH11-2 cells. Data were acquired using a FACS Canto II flow cytometer and analyzed using FlowJo software. (E) Transwell migration of AK3G-shV and AK3G-shH11-2 cells stimulated by SDF-1 (150 ng/ml). Cells were incubated in a Transwell plate (5-μm pore size) for 6 h. Transmigrated and nonmigrated cells were counted using a hemacytometer. The values shown are expressed as the mean ± SD of three independent experiments. A P value less than 0.05 indicates statistical significance. (F) Cell motility (i) and protrusion (ii) of AK3G-shV and AK3G-shH11-2 cells stimulated by SDF-1 (150 ng/ml) for 0 to 20 min in a confined space (3 μm in size).

the fluorescent signals of AK3G-shH11-2 cells were weaker than that of AK3G-shV cells in omental adipose tissue (Fig. 5*B*). The reduction of AK3G-shH11-2 cells in omental adipose tissue was further confirmed by competitive engraftment and clonal expansion assay. The amount of PCR product derived from AK3G-shH11-2 cells was less than AK3G-shV cells in omental adipose tissue 1 day and 4 weeks post-transplantation (Fig. 5*C*). Our results revealed that silencing *Hoxa11* of AK3G cells enhances cell migration through the adipocyte septa of omental adipose tissue or the endothelium of blood vessels.

In a previous study, we generated *Hoxa11*-overexpressing 12G cells (12G-H11-1) by retroviral transduction of full-length *Hoxa11* into 12G cells [24]. BM transplantation assay analysis revealed that mice transplanted with 12G-H11-1 cells, similar to control 12G-V1 cells, did not induce MS formation [24]. However, *in vivo* imaging cell trafficking analysis revealed that strong fluorescent signals of 12G-H11-1 cells were detected in omental adipose tissue 5 min and 1.5 h post-transplantation with the strength of the signals reduced after 24 h, whereas low fluorescent signals of 12G-V1 cells were detected at all time points (Supplementary Fig. 2*A*). Data of competitive engraftment and clonal expansion assay showed that 12G-H11-1 cells were the major cells located in omental and gonadal adipose tissue after 24 h (Supplementary Fig. 2*B*), further supporting that *Hoxa11* reduces leukemia cell migration through adipocyte septa or endothelium and prolongs cell retention in adipose tissues.

Cxcr4/SDF-1 axis-induced cell polarization plays a critical role in hematopoietic stem cell and leukemia cell migration and homing to BM [29,30]. However, flow cytometry analysis showed no significant differences in Cxcr4 expression levels between AK3G-shV and AK3G-shH11-2 cells (Fig. 5*D*), suggesting *Hoxa11*-induced reduction in cell migration was not via reducing of Cxcr4/SDF-1 interaction. Next, we compared cell migration between AK3G-shV and AK3G-shH11-2 cells using SDF-1-stimulated transwell migration assay. Our data showed a 29.7% increase by AK3G-shH11-2 cells in transwell migration through a membrane with 5 μm pores (Fig. 5*E*). Under confined spaces (3 μm in size) with SDF-1-stimulated directional migration, the moving distance of AK3G-shH11-2 cells was significantly further than AK3G-shV cells (Fig. 5F-i). Additionally, protrusion of AK3G-shH11-2 cells was more active than that of AK3G-shV cells (Fig. 5, *F*-ii). These results indicated that *Hoxa11* expression in AK3G cells reduces cell migration and prolongs cell retention in adipose tissue, at least partly, by reducing cell motility and protrusion.

Discussion

The molecular mechanism of MS formation has not been thoroughly investigated. In a previous study, we demonstrated that the upregulation of *Adgra3* (previously named *Gpr125*) in leukemia cells harboring *MLL/AF10* and $KRAS^{G12C}$ enhanced homotypic cell-cell adhesion *in vitro* and MS formation *in vivo* [13]. In this study, we demonstrated that the upregulation of *Hoxa11* in leukemia cells enhanced cell retention in omental adipose tissue and MS formation *in vivo*. Data of SDF-1-stimulated directional transwell migration and cell motility in confined spaces revealed that *Hoxa11* expression reduced leukemia cell migration and protrusion. Furthermore, the observed reduction in cell motility in leukemia cells was not via reducing of SDF-1/Cxcr4 interaction. These results indicate that MS formation is associated with increased cell-cell adhesion and reduced migration of leukemia cells.

To our knowledge, there is no report linking *HOXA11* with cell migration in hematopoietic malignancies. However, the effect of *HOXA11* on cell migration was recurrently reported in solid tumor cells, but with controversial results. *HOXA11* overexpression reduces tumor cell migration in endometrial cancer and renal cell carcinoma [31,32], but enhances tumor cell migration in gastric and breast cancer cells [33,34]. These data indicated that *HOXA11* exhibits positive or negative control on migration is depending on the context of tumor cell type. Further studies are needed to reveal *Hoxa11*-mediated diverse mechanisms underlying cell migration. During cell migration, the first step of the process is the formation of cell protrusions, including actin polymerization-driven lamellipodia and contractility-driven blebs [35]. Among the 77 DEGs identified in this study, 6 genes (*Gas7, Hck, Msrb1, Myo1f, Pls1*, and *Csf1r*) were mapped to GO_BP terms related to actin filament/bundle polymerization or positive regulation of actin cytoskeleton reorganization (Supplementary Table 1). All of these genes were downregulated in MS-inducing AK2G and AK3G cells (Fig. 2*A*). Whether the downregulation of these genes affects actin polymerization-driven lamellipodia and contractility-driven bleb formation and whether these genes are regulated by *Hoxa11* need further investigation.

In this study, we demonstrated that silencing *Hoxa10*, but not *Hoxa11*, in AK3G cells prolonged the survival of recipient mice (Figs. 3*D* and 4*D*). Our results support the clinical observations that *Hoxa10* overexpression is associated with poor prognosis [18,19]. However, in a previous study, we showed that silencing *Hoxa11* expression in *MLL/AF10(OM-LZ)* leukemia cells harboring $PTPN11^{G503A}$ (APm-1) prolonged the survival of recipient mice [24]. These contradictory results may be due to differences in the knockdown efficiency of *Hoxa11* in APm-1 and AK3G leukemia cells. In *Hoxa11* knockdown APm-1 cells (APm-1-shH11-2), *Hoxa11* expression was reduced to the level of cells harboring $PTPN11^{wt}$ (APw-1 cells). In contrast, gene expression was only partially reduced in *Hoxa11* knockdown AK3G cells (Fig. 4, *A–B*). Therefore, we cannot exclude the possibility that *Hoxa11* expression is also critical for the survival of AK3G leukemic mice. MS is considered a poor prognostic factor in AML. Although our results showed that mice transplanted with *Hoxa11* knockdown AK3G cells had reduced MS formation, it did not influence survival compared to those transplanted with control cells (Table 1). Based on the same reason, we cannot exclude the possibility that MS formation is correlated with survival in our mouse model.

Our results showed that ectopic expression of *Hoxa11* in 12G-H11 cells did not induce MS formation in omental adipose tissue, suggesting *Hoxa11* alone is insufficient to induce MS formation. More studies are needed to clarify the biological pathway and the molecular mechanism of *Hoxa11*, as well as *Adgra3*, in MS formation, which may contribute to the development of new targeted therapies to treat patients with AML and MS.

Supplementary Figure 1. Cooperation of *MLL/AF10(OM-LZ)* with $KRAS^{G12C}$-induced myeloid leukemia with shorter latency and induced MS formation at extramedullary sites. (*A*) Flowchart for establishing the *MLL/AF10(OM-LZ)* cell line (12G) and the *MLL/AF10(OM-LZ)* cell lines harboring $KRAS^{wt}$ (AKw1G) or oncogenic $KRAS^{G12C}$ (AK2G, AK3G, and AK5G). (*B*) Kaplan–Meier survival curves of mice ip injected with AKw1G (n = 5) and AK5G (n = 5) cells. Mice ip injected with normal saline served as a blank control. (*C*) Gross view of excised GI-OM adipose tissue from blank, AKw1G, and AK5G mice. Arrows indicate tumor masses.

Supplementary Figure 2. Ectopic expression of *Hoxa11* in 12G cells prolonged cell retention in adipose tissue. (*A*) Imaging analysis of mice ip injected with CellVue NIR815-labeled AK3G-shV or AK3G-shH11-2 cells by Peral Imager at indicated time points. Mice were under anesthesia during image capture. (*B*) *In vivo* competitive engraftment and clonal expansion analysis of 12G-V and 12G-H11 cells in OM and Go adipose tissues of recipient mice on the first day. 12G-V and 12G-H11 cells were initially mixed in a 1:1 ratio by cell number. The arrowhead indicates the 62nd nucleotide (C for 12G-H11 and G for 12G-V).

Declaration of Competing Interest

The authors declare no competing financial interests.

CRediT authorship contribution statement

Jen-Fen Fu: Conceptualization, Data curation, Funding acquisition, Investigation, Methodology, Project administration, Validation, Writing – original draft. **Chih-Jen Wen:** Methodology, Data curation, Formal analysis, Visualization. **Tzung-Hai Yen:** Methodology, Software, Visualization. **Lee-Yung Shih:** Conceptualization, Data curation, Resources, Writing – review & editing.

Acknowledgments

This work was supported by grants from the Ministry of Science and Technology (107-2320-B-182A-013) and the Chang Gung Memorial Hospital (CMRPG3E1391-3, CMRPG3G1821, and CMRPG3J1331), Taiwan. We thank Mrs. Jun-Wei Huang and Chih-Shien Chuang for technical assistance in all experiments.

References

[1] Magdy M, Abdel Karim N, Eldessouki I, Gaber O, Rahouma M, Ghareeb M. Myeloid Sarcoma. *Oncology Research and Treatment* 2019;**42**:219–24.

[2] Shahin OA, Ravandi F. Myeloid sarcoma. *Current Opinion in Hematology* 2020;**27**.

[3] Bakst RL, Tallman MS, Douer D, Yahalom J. How I treat extramedullary acute myeloid leukemia. *Blood* 2011;**118**:3785–93.

[4] Goyal G, Bartley AC, Patnaik MM, Litzow MR, Al-Kali A, Go RS. Clinical features and outcomes of extramedullary myeloid sarcoma in the United States: analysis using a national data set. *Blood Cancer Journal* 2017;**7**:e592.

[5] Pileri SA, Ascani S, Cox MC, et al. Myeloid sarcoma: clinico-pathologic, phenotypic and cytogenetic analysis of 92 adult patients. *Leukemia* 2007;**21**:340–50.

[6] Claerhout H, Van Aelst S, Melis C, et al. Clinicopathological characteristics of de novo and secondary myeloid sarcoma: A monocentric retrospective study. *European Journal of Haematology* 2018;**100**:603–12.

[7] Ullman DI, Dorn D, Jones JA, et al. Clinicopathological and molecular characteristics of extramedullary acute myeloid leukaemia. *Histopathology* 2019;**75**:185–92.

8 Byrd JC, Weiss RB, Arthur DC, et al. Extramedullary leukemia adversely affects hematologic complete remission rate and overall survival in patients with t(8;21)(q22;q22): results from Cancer and Leukemia Group B 8461. *Journal of Clinical Oncology* 1997;**15**:466–75.

[9] Stove HK, Sandahl JD, Abrahamsson J, et al. Extramedullary leukemia in children with acute myeloid leukemia: A population-based cohort study from the Nordic Society of Pediatric Hematology and Oncology (NOPHO). *Pediatric Blood & Cancer* 2017;**64**.

[10] Pastoret C, Houot R, Llamas-Gutierrez F, et al. Detection of clonal heterogeneity and targetable mutations in myeloid sarcoma by high-throughput sequencing. *Leukemia & Lymphoma* 2017;**58**:1008–12.

[11] Choi M, Jeon YK, Sun CH, et al. RTK-RAS pathway mutation is enriched in myeloid sarcoma. *Blood Cancer Journal* 2018;**8**:43.

[12] Kashofer K, Gornicec M, Lind K, et al. Detection of prognostically relevant mutations and translocations in myeloid sarcoma by next generation sequencing. *Leukemia & Lymphoma* 2018;**59**:501–4.

[13] Fu JF, Yen TH, Chen Y, et al. Involvement of Gpr125 in the myeloid sarcoma formation induced by cooperating *MLL/AF10(OM-LZ)* and oncogenic *KRAS* in a mouse bone marrow transplantation model. *International Journal of Cancer* 2013;**133**:1792–802.

[14] Yu BD, Hess JL, Horning SE, Brown GA, Korsmeyer SJ. Altered Hox expression and segmental identity in Mll-mutant mice. *Nature* 1995;**378**:505–8.

[15] Mohi MG, Williams IR, Dearolf CR, et al. Prognostic, therapeutic, and mechanistic implications of a mouse model of leukemia evoked by Shp2 (PTPN11) mutations. *Cancer Cell* 2005;**7**:179–91.

[16] Martino V, Bianchera A, Reia L, et al. Down-regulation of HOXA4, HOXA7, HOXA10, HOXA11 and MEIS1 during monocyte-macrophage differentiation in THP-1 cells. *Molecular Medicine Reports* 2009;**2**:241–4.

[17] Coenen EA, Zwaan CM, Reinhardt D, et al. Pediatric acute myeloid leukemia with t(8;16)(p11;p13), a distinct clinical and biological entity: a collaborative study by the International-Berlin-Frankfurt-Münster AML-study group. *Blood* 2013;**122**:2704–13.

[18] Guo C, Ju QQ, Zhang CX, Gong M, Li ZL, Gao YY. Overexpression of HOXA10 is associated with unfavorable prognosis of acute myeloid leukemia. *BMC Cancer* 2020;**20**:586.

[19] Nagy Á, Őcsz Á, Budczies J, et al. Elevated HOX gene expression in acute myeloid leukemia is associated with NPM1 mutations and poor survival. *Journal of Advanced Research* 2019;**20**:105–16.

[20] Thorsteinsdottir U, Sauvageau G, Hough MR, et al. Overexpression of HOXA10 in murine hematopoietic cells perturbs both myeloid and lymphoid differentiation and leads to acute myeloid leukemia. *Molecular and Cellular Biology* 1997;**17**:495–505.

[21] Fujino T, Suzuki A, Ito Y, et al. Single-translocation and double-chimeric transcripts: detection of NUP98-HOXA9 in myeloid leukemias with HOXA11 or HOXA13 breaks of the chromosomal translocation t(7;11)(p15;p15). *Blood* 2002;**99**:1428–33.

[22] Mizoguchi Y, Fujita N, Taki T, Hayashi Y, Hamamoto K. Juvenile myelomonocytic leukemia with t(7;11)(p15;p15) and NUP98-HOXA11 fusion. *American Journal of Hematology* 2009;**84**:295–7.

[23] Fu JF, Hsu CL, Shih LY. *MLL/AF10(OM-LZ)*-immortalized cells expressed cytokines and induced host cell proliferation in a mouse bone marrow transplantation model. *International Journal of Cancer* 2010;**126**:1621–9.

[24] Fu JF, Shih LY, Yen TH. HOXA11 plays critical roles in disease progression and response to cytarabine in AML. *Oncology Reports* 2021;**46**.

[25] Fu J-F, Yen T-H, Huang Y-J, Shih L-Y. Ets1 Plays a Critical Role in MLL/EB1-Mediated Leukemic Transformation in a Mouse Bone Marrow Transplantation Model. *Neoplasia* 2019;**21**:469–81.

[26] Livak KJ, Schmittgen TD. Analysis of relative gene expression data using real-time quantitative PCR and the 2(-Delta Delta C(T)) Method. *Methods* 2001;**25**:402–8.

[27] Fu J-F, Liang S-T, Huang Y-J, et al. Cooperation of *MLL/AF10(OM-LZ)* with PTPN11 activating mutation induced monocytic leukemia with a shorter latency in a mouse bone marrow transplantation model. *International Journal of Cancer* 2017;**140**:1159–72.

[28] Lavenus SB, Tudor SM, Ullo MF, Vosatka KW, Logue JS. A flexible network of vimentin intermediate filaments promotes migration of amoeboid cancer cells through confined environments. *The Journal of Biological Chemistry* 2020;**295**:6700–9.

[29] Kollet O, Spiegel A, Peled A, et al. Rapid and efficient homing of human CD34+CD38−/lowCXCR4+stem and progenitor cells to the bone marrow and spleen of NOD/SCID and NOD/SCID/B2mnull mice. *Blood* 2001;**97**:3283–91.

[30] Burger JA, Bürkle A. The CXCR4 chemokine receptor in acute and chronic leukaemia: a marrow homing receptor and potential therapeutic target. *British Journal of Haematology* 2007;**137**:288–96.

[31] Wang L, Cui Y, Sheng J, et al. Epigenetic inactivation of HOXA11, a novel functional tumor suppressor for renal cell carcinoma, is associated with RCC TNM classification. *Oncotarget* 2017;**8**:21861–70.

[32] Kong C, Zhu Z, Li Y, Xue P, Chen L. *Downregulation of HOXA11 enhances endometrial cancer malignancy and cisplatin resistance via activating PTEN/AKT signaling pathway*. Clinical & translational oncology: official publication of the Federation of Spanish Oncology Societies and of the National Cancer Institute of Mexico; 2021.

[33] Wang C, Shi M, Ji J, et al. A self-enforcing HOXA11/Stat3 feedback loop promotes stemness properties and peritoneal metastasis in gastric cancer cells. *Theranostics* 2019;**9**:7628–47.

[34] Sun Y, Zeng C, Gan S, et al. LncRNA HOTTIP-Mediated HOXA11 Expression Promotes Cell Growth, Migration and Inhibits Cell Apoptosis in Breast Cancer. *International Journal of Molecular Sciences* 2018;**19**:472.

[35] Bergert M, Chandradoss SD, Desai RA, Paluch E. Cell mechanics control rapid transitions between blebs and lamellipodia during migration. In: *Proceedings of the National Academy of Sciences*, 109; 2012. p. 14434–9.